

Article

# Thermal Transformation of $\text{NH}_4$ -Clinoptilolite to Mullite and Silica Polymorphs

Antonio Brundu, Guido Cerri \* and Eleonora Sale

Department of Natural and Territorial Sciences, University of Sassari, Via Piandanna 4, 07100 Sassari, Italy; abrundu@uniss.it (A.B.); eleonorasale@hotmail.it (E.S.)

\* Correspondence: gcerri@uniss.it; Tel.: +39-079-228621

Academic Editor: Annalisa Martucci

Received: 14 December 2016; Accepted: 13 January 2017; Published: 19 January 2017

**Abstract:** Clinoptilolite is a natural zeolite used for the abatement of ammonium in the treatment of urban wastewater. By considering that mullite was obtained through thermal treatment of  $\text{NH}_4$ -exchanged synthetic zeolites, this work aimed to evaluate if this phase can be obtained from  $\text{NH}_4$ -clinoptilolite. A material containing about 90 wt % of clinoptilolite, prepared using a Sardinian zeolite-rich rock, was  $\text{NH}_4$ -exchanged and subjected to treatments up to 1200 °C. After dehydration, de-ammoniation, and dehydroxylation processes, the clinoptilolite structure collapsed at 600 °C. An association of mullite, silica polymorphs, and glass, whitish in color, was obtained for treatments between 1000 and 1200 °C. The higher degree of crystallinity was reached after a 32 h heating at 1100 °C: mullite 22 wt %, cristobalite 59 wt %, tridymite 10 wt %, glass 9 wt %. It is possible to speed up the kinetics of the transformation by increasing the temperature to 1200 °C, obtaining the same amount of mullite in 2 h, but increasing the residual amorphous fraction (16 wt %). These results indicate that  $\text{NH}_4$ -clinoptilolite could represent a raw material of potential interest in the ceramic field, in particular in the production of acid refractory, opening scenarios for a possible reuse of clinoptilolite-based exchangers employed in ammonium decontamination.

**Keywords:** zeolite; clinoptilolite; mullite; ammonium; ammonia; cristobalite; ceramic; refractory; thermal treatment; waste

## 1. Introduction

Clinoptilolite is the most abundant among natural zeolites and high-grade deposits are distributed worldwide [1]. Not only has it cation exchange capacity, but it also exhibits high selectivity toward  $\text{NH}_4^+$ , known since the sixties of the past century, when the first studies, addressed to exploit this feature in the treatment of municipal wastewater, were accomplished [2]. However, the use of clinoptilolite in ammonium decontamination still remains a matter of interest [3–5]. In the United States, nearly 80% of the zeolites sold in the domestic market is related to uses exploiting ammonia/ammonium adsorption, such as animal feed, odor control, water purification, pet litter, and wastewater treatment [6]; noteworthy, clinoptilolite represents more than 85% of US production [7]. Clinoptilolite has been employed in the treatment of urban wastewater for the removal of  $\text{NH}_4^+$  [1,8], also taking advantage of its low cost, although only a limited number of plants, three in the USA and fourteen in Australia, have operated [1]. It should be noted that the regeneration of the exhausted zeolite, as well as the recovery of ammonia, are feasible processes, but often not cost-effective [9]. This general rule has resulted in being pushed to find uses for the spent exchangers, for example clinoptilolite containing ammonium ions can be used as fertilizer [8], and should encourage further studies aimed to evaluate new alternatives.

Heating determines transformations in the structure of zeolites, and some general rules governing the correlation between the composition, original framework, and the thermal stability of these minerals

have been established [10]. It has been demonstrated that some  $\text{NH}_4$ -exchanged synthetic zeolites can be transformed into an association of mullite and amorphous silica by thermal treatments [11–13]. Mullite has achieved outstanding importance as a material for both traditional and advanced ceramics because of its favorable thermal and mechanical properties [14]. The use of natural zeolites in ceramic production has been evaluated by different research groups, highlighting the advantages, generally a lowering of sintering temperatures and limits, mainly linked to the dark color often observed in the fired products [15–19]. Recent papers show that crystalline materials can be obtained by thermally induced transformation of Cs- and Pb-exchanged clinoptilolite [20–22], whereas only an amorphous phase has been achieved from the thermal treatment of a  $\text{NH}_4$ -clinoptilolite [23].

The continuous increase of quantity of inorganic waste has stimulated, as a challenge, different studies designed to transform waste into resources for the ceramic industry [24–26]. With this perspective, a material containing  $\text{NH}_4$ -clinoptilolite, derived from a wastewater treatment, might be evaluated as a potential raw material for the ceramic industry. On the basis of the above mentioned considerations, the present research has been addressed to evaluate the possibility of obtaining a ceramic matrix by heating an  $\text{NH}_4$ -exchanged clinoptilolite.

## 2. Experimental Section

### 2.1. Starting Material and Beneficiation Process

The present research was performed by using a clinoptilolite-bearing epiclastite (sample labeled as “LacBen”) [27], collected in the valley of the Tirso River (Northern Sardinia, Italy). Literature data report zeolite contents that span from 66 to 70 wt % for this material [22,28].

The rock was subjected to the beneficiation process described in previous papers [20,22,29,30], aimed to increase the zeolite content. Briefly, the material was submitted to autogenous comminution and dry sieving. Then, the fraction below 100  $\mu\text{m}$  was subjected to ultrasound attack and wet separation in deionized water. The obtained powder was dried at 70 °C in a ventilated drying oven, then conditioned for 24 h at  $22 \pm 3$  °C and  $53\% \pm 5\%$  of Relative Humidity (hereafter, RH), monitored with an Ebro Data Logger EBI20-TH1 (Ebro, Ingolstadt, Germany), using a desiccator containing a saturated solution of  $\text{Ca}(\text{NO}_3)_2$ . The material so obtained was labeled ES-AR.

### 2.2. Preparation of $\text{NH}_4$ -Clinoptilolite

To obtain a  $\text{NH}_4$ -clinoptilolite, ES-AR was previously Na-exchanged, a procedure that allows an improvement of the cation exchange capacity [31]. The enriched powder was contacted with a 1 M NaCl solution (Merck ACS salt; purity > 99.5%) performing a sequence of ten exchange cycles of 2 h each, executed in a batch at 65 °C under continuous stirring, with a solid/liquid ratio of 30 g/L. The last two exchange cycles were performed using a VWR Prolabo salt (purity 99.9%). The Na-exchanged material was rinsed with deionized water until complete removal of chloride solution (test performed on elutes with  $\text{AgNO}_3$ ). The powder was dried at 35 °C overnight, then rehydrated for 24 h at 22 °C and  $53\% \pm 2\%$  of RH. The Na-clinoptilolite was conducted in  $\text{NH}_4$ -form using a 0.5 M  $\text{NH}_4\text{Cl}$  solution (Sigma Aldrich salt; purity 99.5%), by carrying out five exchange cycles using the same conditions of Na-preconditioning. Once rinsed, the material was dried and rehydrated as described above. The  $\text{NH}_4$ -exchanged material was labeled ES-NH.

### 2.3. Chemical Analysis

The chemical analysis of ES-NH was performed at the Activation Laboratories Ltd (Ancaster, ON, Canada). Major elements were determined after lithium metaborate/tetraborate fusion of the sample through Inductive Coupled Mass Atomic Emission Spectrometry (ICP-AES), performed with a Varian Vista 735 ICP (Varian, Inc., Palo Alto, CA, USA).  $\text{NH}_4$  content was calculated on the basis of the Total N determined through the Total Kjeldahl Nitrogen (TKN) method. The Loss of Ignition (LoI) of the material was determined, in duplicate, by calcination of the sample for 2 h at 1000 °C. The  $\text{H}_2\text{O}$

content in the  $\text{NH}_4$ -clinoptilolite was calculated as the difference between the LoI and the  $(\text{NH}_4)_2\text{O}$  content [32].

#### 2.4. Thermal Treatments

Aliquots of 250 mg of ES-NH were submitted to thermal treatments of 2 h at 200, 300, 400, 500, 600, 700, 800, 900, 1000, 1100, and 1200 °C, performed in a muffle furnace (Vittadini mod. FS. 3, Vittadini, Milano, Italy) using platinum crucibles. Further experiments were performed at 1000 and 1100 °C, at each temperature heating aliquots of 250 mg of sample for 4, 8, 16, and 32 h.

#### 2.5. X-ray Diffraction (XRD)

ES-AR, ES-NH, and all heated samples were investigated employing a Bruker D2-Phaser (Bruker, Karlsruhe, Germany) with the following conditions: 30 kV, 10 mA,  $\text{CuK}\alpha$  radiation, LynxEye detector with an angular opening of 5°,  $2\theta$  range 6°–70°, step size 0.020°, time per step 2 s, spinner 15 rpm. Before the measurements, all the samples were micronized using a Retsch MM400 mill ( $\text{ZrO}_2$  cups and balls). ES-AR, ES-NH heated for 32 h at 1000 and 1100 °C, and ES-NH heated for 2 h at 1200 °C were also analyzed by adding to the specimens 20 wt % of corundum as internal standard. All measurements were performed using a low-background silicon crystal specimen holder (Bruker), except for the ES-AR, placed in a steel sample holder (Bruker). The XRD patterns were evaluated using the software EVA 4.1.1 (2015; Bruker DIFFRACplus Package) coupled with the database PDF-2 (ICDD). Quantitative analyses were performed with the Rietveld method using the software Bruker Topas 4.5.

#### 2.6. Thermal Analyses

Thermogravimetric, Derivative Thermogravimetric and Differential Thermal Analyses (hereafter, TG, DTG, and DTA) of ES-NH were carried out using a TA Instrument Q600 (TA Instruments, New Castle, DE, USA) simultaneous thermal analyzer. Amounts of about 15 mg of sample were heated up to 1300 °C, both under air (five analyses) and nitrogen flow (one analysis;  $\text{N}_2$  purity 99.999%, Sapio), in an alumina crucible at the following operating conditions: 10 °C/min; gas flow 100 mL/min. The software TA-Universal Analysis was used to evaluate the results.

#### 2.7. Scanning Electron Microscope (SEM) Observations

Morphological observations were carried out on the samples heated for 32 h at 1100 °C and for 2 h at 1200 °C. The materials, placed on aluminum stubs, were gold coated by sputtering and observed using a ZEISS DSM 962 Scanning Electron Microscope (Zeiss, Oberkochen, Germany).

### 3. Results

The mineralogical composition of ES-AR is reported in Table 1 (the Rietveld refinement is provided in Figure S1, Supplementary Materials). The beneficiation process enabled a powder to be obtained with a clinoptilolite content of about 89 wt %, along with residual amounts of feldspars, glass, opal-CT, biotite, and quartz. This result confirms that the beneficiation process here adopted is effective and replicable [20,22,29,30].

**Table 1.** Mineralogical composition of sample ES-AR (values in wt %; e.s.d. = estimated standard deviation; R-weighted pattern (Rwp) = 6.96%).

ES-AR	Clinoptilolite	Feldspars	Quartz	Opal-CT	Biotite	Amorphous	Sum
<b>content</b>	89.3	4.0	0.7	2.1	1.0	2.9	100.0
<b>e.s.d.</b>	±4.0	±1.0	±0.2	±0.5	±0.2	±1.2	-

The chemical composition of ES-NH is reported in Table 2.

**Table 2.** Chemical composition of sample ES-NH (values in wt %).

SiO <sub>2</sub>	Al <sub>2</sub> O <sub>3</sub>	Fe <sub>2</sub> O <sub>3</sub>	MnO	MgO	CaO	Na <sub>2</sub> O	K <sub>2</sub> O	TiO <sub>2</sub>	P <sub>2</sub> O <sub>5</sub>	(NH <sub>4</sub> ) <sub>2</sub> O	H <sub>2</sub> O	Sum
67.85	12.81	0.78	0.01	0.39	0.30	0.14	0.46	0.23	0.05	5.76	10.92	99.70

The high ammonium content (2.21 meq/g), along with the low sodium, potassium, calcium, and magnesium contents, indicate that a near end-member of NH<sub>4</sub>-clinoptilolite was obtained.

The XRD patterns of ES-NH and of all the samples heated for 2 h from 200 to 1200 °C are reported in Figure 1. The diffractograms show that the structure of clinoptilolite is well recognizable also after the treatment at 500 °C, although a slight shifting of the peaks toward higher 2θ angles, and a reduction of their intensities, occurred. The heating at 600 °C determined the amorphization of the material (Figure 1a), and no further change was recorded up to 1000 °C, when the nucleation of cristobalite began (Figure 1b). The XRD pattern of ES-NH treated at 1100 °C shows, beside cristobalite, also traces of tridymite and mullite.

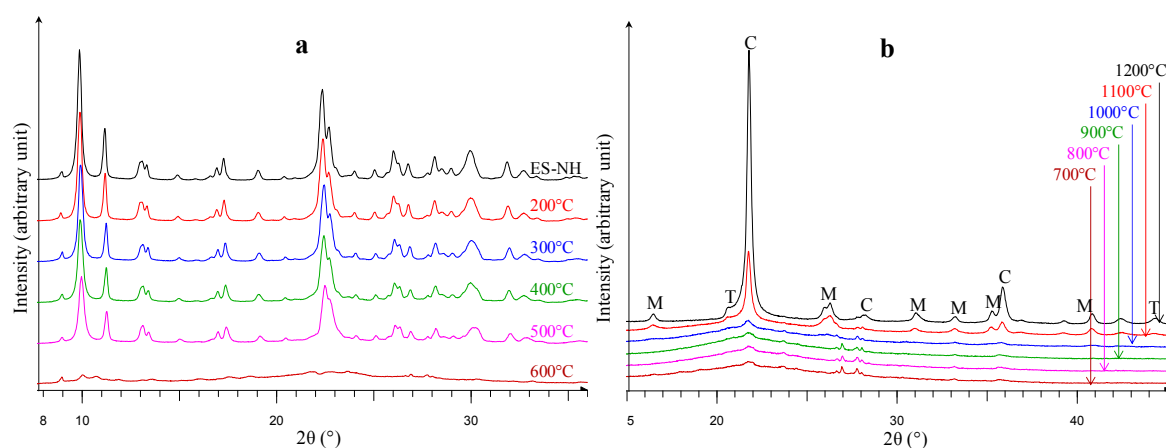


**Figure 1.** (a) X-ray Diffraction (XRD) patterns of ES-NH unheated and treated for 2 h from 200 to 600 °C and; (b) from 700 to 1200 °C. C = Cristobalite; M = Mullite; T = Tridymite.

At 1200 °C, a matrix almost entirely crystalline, basically composed of cristobalite (54.3 wt %), tridymite (8.8 wt %) and mullite (21.0 wt %), was obtained (Figure 1b and Table 3).

**Table 3.** Mineralogical compositions of ES-NH heated at the temperatures and for the time indicated (values in wt %).

Temperature	Time (h)	Cristobalite	Tridymite	Mullite	Amorphous	Sum	Rwp
1000 °C	32	5.1	3.5	5.2	86.2	100.0	3.91
e.s.d.	-	±1.0	±0.7	±1.0	±6.0	-	-
1100 °C	32	59.3	10.1	21.8	8.8	100.0	7.97
e.s.d.	-	±2.8	±1.6	±1.8	±2.0	-	-
1200 °C	2	54.3	8.8	21.0	15.9	100.0	8.18
e.s.d.	-	±2.5	±1.4	±1.8	±2.5	-	-

The XRD patterns of the ES-NH heated up to 32 h at 1000 and 1100 °C are reported in Figure 2. In both cases the crystallization increases with the time, but very slowly at 1000 °C, indeed after 32 h the amorphous phase is largely dominant (about 86 wt %—Table 3). Conversely, the residual glassy fraction is just 8.8 wt % in the sample heated at 1100 °C for 32 h, that is mainly composed of cristobalite (about 59 wt %) and mullite (almost 22 wt %), as reported in Table 3 (the Rietveld refinement is

provided in Figure S2, Supplementary Materials). A thermal treatment at 1200 °C allows 21 wt % of mullite to be obtained in just 2 h, but in this case the amorphous fraction reaches 16 wt % (Table 3).

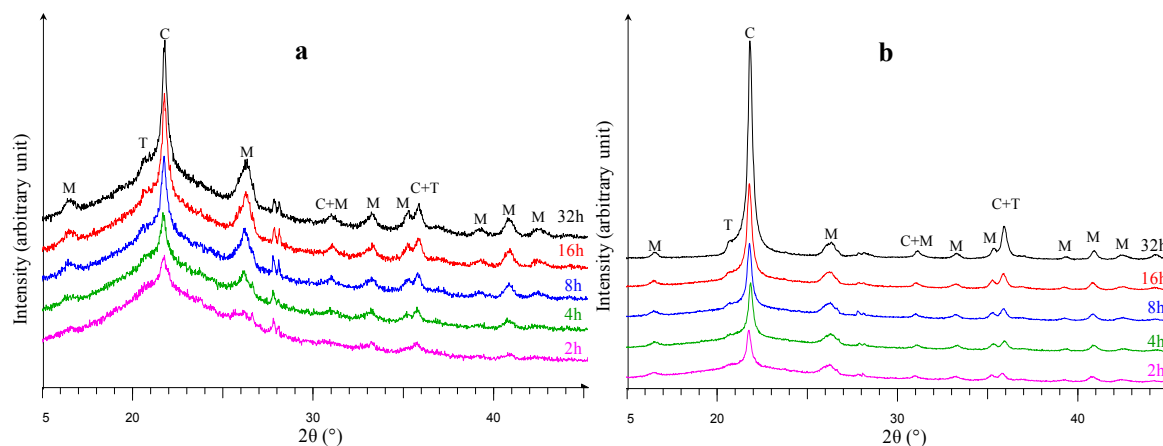


**Figure 2.** (a) XRD patterns of ES-NH treated up to 32 h at 1000; and (b) at 1100 °C. C = Cristobalite; M = Mullite; T = Tridymite.

The results of the thermal analyses of ES-NH are reported in Figure 3. The weight loss occurred in four steps, well-marked in the DTG curves. Except for the slight offset of the last weight loss, the TG and DTG curves follow the same paths, regardless of the gas used during the analysis; no mass loss was recorded above 800 °C. Besides the endothermic peaks associated to the weight losses, the DTA curves show three exothermic reactions, at 550, 1041, and 1149 °C when the sample was analyzed under an air flow, and at 577, 1014, and 1148 °C in a nitrogen atmosphere. Finally, both DTA curves exhibit a broad endotherm at about 1200 °C.

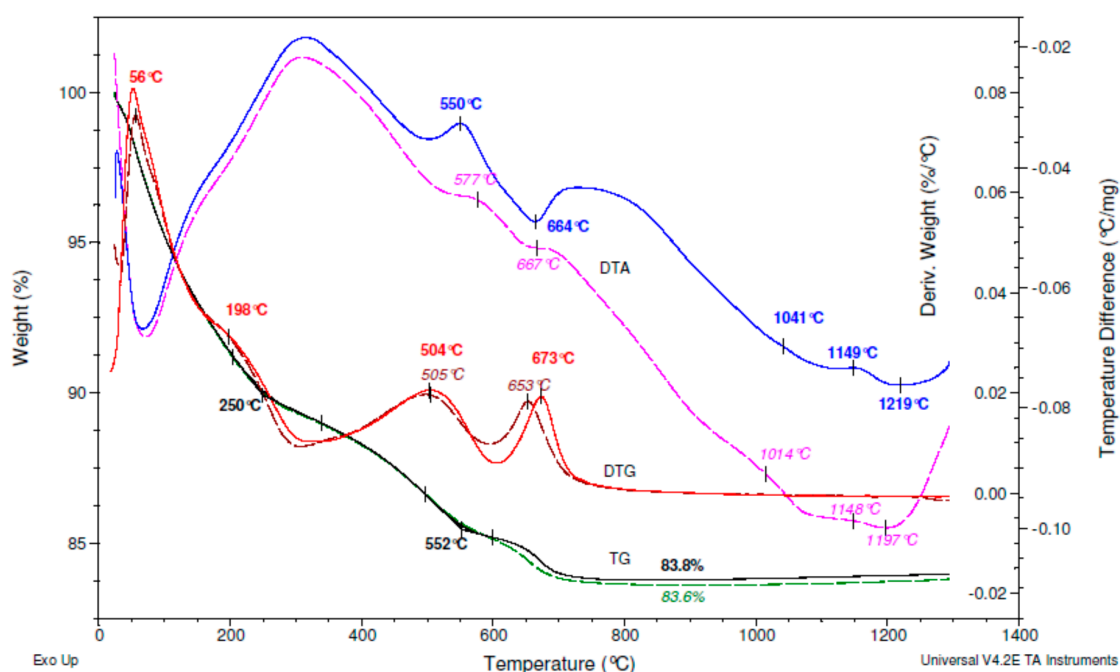


**Figure 3.** Thermogravimetric, Derivative Thermogravimetric, and Differential Thermal Analyses (TG-DTG-DTA) curves of ES-NH analyzed under flow of air (solid lines) or nitrogen (dashed lines).

SEM observations performed on ES-NH heated at 1200 °C evidenced rounded grains, often coalescent (Figure 4a); at higher magnification, the presence of acicular shapes (about 1 μm

in length) can be inferred (Figure 4b). These morphologies were not noticed in the sample treated at 1100 °C for 32 h.

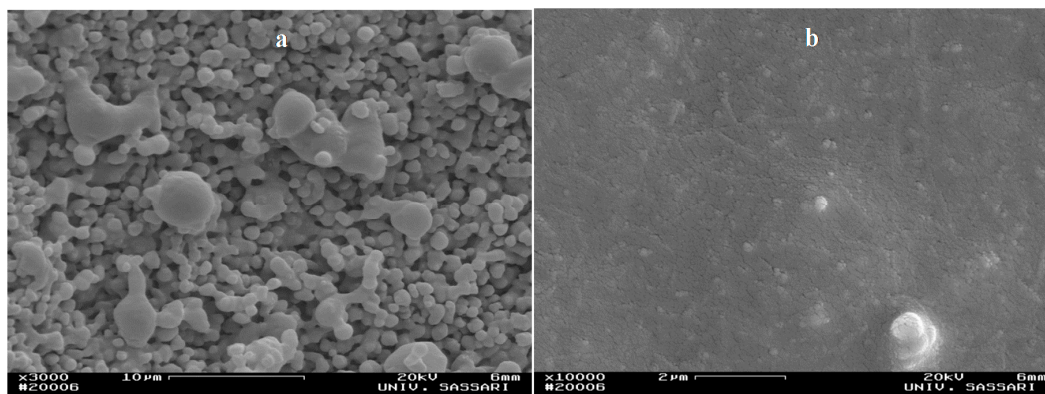


**Figure 4.** Scanning electron microscopy (SEM) images of ES-NH heated at 1200 °C.

#### 4. Discussion

In discussing the phenomena occurring during the heating of ES-NH it is appropriate to start with the thermal analysis, and compare the results with those reported by Tomazovic et al. [32] in their detailed study on the properties of a Serbian clinoptilolite conducted in  $\text{NH}_4$ -form. In Figure 3, the peaks marked on the DTG curve at 56 and 198 °C are related to the loss of water. At about 250 °C the material starts to evolve  $\text{NH}_3$ , a process that overlaps to the residual dehydration still in progress. From the kinetic point of view, the weight loss associated with ammonia release reaches the maximum at about 500 °C (see DTG), and this process ends at about 550 °C (see offset on the TG curve), substantially in agreement with the data in the literature [32]. A heating time of 2 h at 500 °C should have been sufficient to evolve all the ammonia contained in ES-NH, hence the corresponding XRD pattern in Figure 1a can be attributed to an H-form of clinoptilolite [33]. The slight shifting of several peaks toward higher  $2\theta$  angles, observable by comparing the XRD patterns of ES-NH heated up to 500 °C (Figure 1a), is compatible with a progressive reduction of the cell volume of clinoptilolite, determined by the dehydration and de-ammoniation processes [32].

The exothermic peak at 550 °C along the DTA path in Figure 3 (see analysis under air flow), is related to the combustion of the ammonia released from the zeolite. In air, this phenomenon should take place at 651 °C, but clinoptilolite (like other zeolites) can catalyze the auto-ignition of ammonia, triggering this process already at 530–570 °C [32,34]. When the analysis was performed under a flow of nitrogen, because of the reduced availability of oxygen inside the furnace, the exothermic peak of ammonia combustion showed weaker intensity, and a shift of almost 30 °C toward higher temperatures (Figure 3).

The DTG curves of ES-NH show a sharp peak at 650–675 °C (Figure 3), linked to the dehydroxylation of the H-clinoptilolite [33]. This weight loss is also marked by an evident endothermic reaction along the DTA paths (at 664–667 °C, Figure 3), and the five analyses performed under air flow showed always the same peaks in the same positions. These DTG/DTA peaks are not present in the thermal analyses of  $\text{NH}_4$ -clinoptilolite previously reported by other authors [32–34]; this may be due to a combination of the following factors: (i) the content of clinoptilolite in the material; (ii) the content of  $\text{NH}_4^+$  in the zeolite; (iii) the performance of the thermal analyzer used. The reaction of dehydroxylation accompanies the collapse of the zeolite framework. In fact after a heating time of 2 h at 600 °C, ES-NH becomes amorphous (Figure 1a), whereas the breakdown of the  $\text{NH}_4$ -clinoptilolite prepared by Tomazovic et al. [23] begins at 600 °C, a difference that can be explained by the higher Si/Al ratio of the Serbian clinoptilolite (5.02) [32] with respect to that of the Sardinian zeolite contained in ES-NH (4.71) [28].

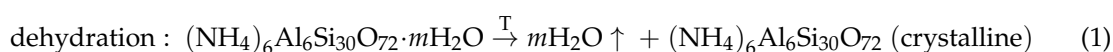
Above 1000 °C, the DTA curves show a first weak exothermic (more difficult to recognize in the analysis performed under air flow) between 1014 and 1041 °C, and a second, clearer, at about 1150 °C (Figure 3). Such peaks are attributable to the nucleation of cristobalite and mullite, respectively, in fact, in the XRD patterns of Figure 1b, the main reflection of the silica polymorph becomes distinguishable after a treatment of 2 h at 1000 °C, whereas the nucleation of mullite required a heating at 1100 °C. The broad endothermic peak along the DTA curves in Figure 3, with a minimum at about 1200 °C, should correspond to the formation of a liquid phase.

The nucleation of cristobalite from thermally treated zeolites is not a novelty [22,23,35] but, so far, it has never been reported for NH<sub>4</sub>-clinoptilolite. An analogous consideration applies to mullite; in fact, literature reports the thermal transformation of NH<sub>4</sub>-exchanged synthetic zeolites to mullite [12,13], but this phase has never been obtained from natural zeolites. It should be noted that Tomazovic et al. [23] heated a NH<sub>4</sub>-clinoptilolite for 2 h at 1100 °C without obtaining mullite or cristobalite.

XRD results summarized in Figure 2 and Table 3 indicate that the kinetic aspects of the transformation from NH<sub>4</sub>-clinoptilolite to mullite and silica polymorphs are relevant. At 1000 °C the reaction proceeds very slowly, remaining largely incomplete after 32 h, whereas with the same time at 1100 °C enabled the best result in terms of crystallinity to be obtained: only 8.8 wt % of amorphous fraction. It is possible to speed up the transformation by increasing the temperature to 1200 °C, but this results in an increase of the residual glassy fraction (15.9 wt %).

With respect to SEM observations performed on ES-NH heated for 2 h at 1200 °C, the shape of the grains and their coalescence could be due to incipient melting (Figure 4a), an hypothesis consistent with the results of thermal analyses, whereas the (rare) needle-like morphologies could correspond to mullite crystals (Figure 4b). In spite of an almost identical mineralogical composition, the sample heated for 32 h at 1100 °C does not show these morphologies, probably because the phase transformations took place in the solid state. On the other hand, this is the case for a material containing 63 wt % of mullite obtained from zeolite A [13], that shows the morphology of the precursor even if the zeolite structure has been destroyed. The phases nucleated from ES-NH cannot inherit the habitus of clinoptilolite because it is destroyed during the enrichment process [20].

Results show that during the heating, but before the nucleation of the high-temperature phases, NH<sub>4</sub>-clinoptilolite undergoes the phenomena summarized by Jacobs et al. [33], here schematized for a clinoptilolite with Si/Al ratio = 5:



Such phenomena, accompanied by the mass losses detected through thermogravimetric analysis (Figure 3), determine a progressive transformation in the chemical composition of ES-NH (Table 4), illustrated by using the M<sub>2</sub>O-Al<sub>2</sub>O<sub>3</sub>-SiO<sub>2</sub> ternary diagram in Figure 5.

**Table 4.** Chemical composition of ES-NH after dehydration (D-1), de-ammoniation (D-2) and dehydroxylation (D-3), with mullite (Mul) composition calculated from the formula Al<sub>6</sub>Si<sub>2</sub>O<sub>13</sub> (wt %).

Sample	SiO <sub>2</sub>	Al <sub>2</sub> O <sub>3</sub>	Fe <sub>2</sub> O <sub>3</sub>	MnO	MgO	CaO	Na <sub>2</sub> O	K <sub>2</sub> O	TiO <sub>2</sub>	P <sub>2</sub> O <sub>5</sub>	M <sub>2</sub> O	Sum
D-1	76.43	14.43	0.88	0.01	0.44	0.34	0.16	0.52	0.26	0.06	6.48 <sup>a</sup>	100.00
D-2	79.81	15.07	0.92	0.01	0.46	0.35	0.17	0.54	0.27	0.06	2.34 <sup>b</sup>	100.00
D-3	81.73	15.43	0.94	0.01	0.47	0.36	0.17	0.56	0.27	0.06	-	100.00
Mul	28.20	71.80	-	-	-	-	-	-	-	-	-	100.00

<sup>a</sup> M corresponds to ammonium; <sup>b</sup> M corresponds to hydrogen.

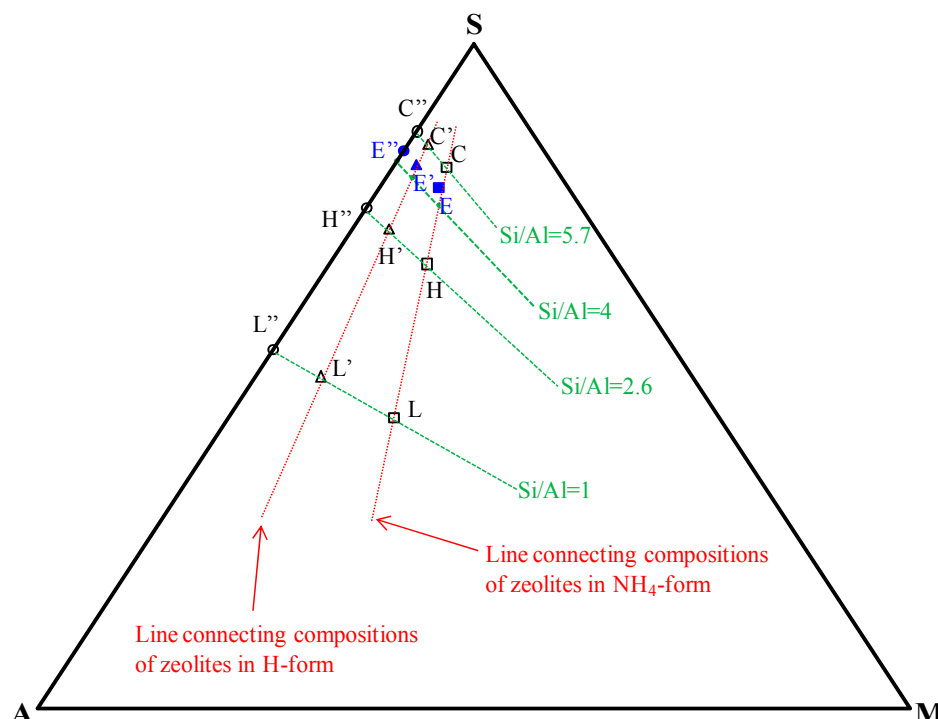


**Figure 5.** Ternary plot for  $M_2O-Al_2O_3-SiO_2$  system (values in wt %). S = silica; A = alumina; M = oxide of ammonium (for square marks) or hydrogen (for triangle marks). C = dehydrated  $NH_4$ -clinoptilolite (Si/Al = 5.7); E = dehydrated ES-NH; H = dehydrated  $NH_4$ -heulandite (Si/Al = 2.6); L = dehydrated  $NH_4$ -LTA zeolite. C', E', H', and L': composition of the same materials after de-ammoniation. C'', E'', H'', and L'': composition of the same materials after dehydroxylation.

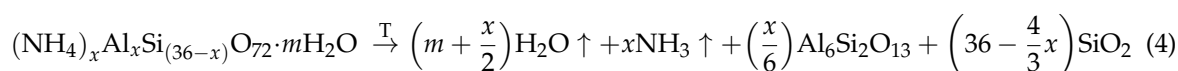
The components of the system are the oxides of: silicon at the vertex S, aluminum at the vertex A, and, at vertex M, alternatively ammonium (for square marks as E, that corresponds to ES-NH dehydrated) or hydrogen (for triangle marks as E', that corresponds to de-ammoniated ES-NH). Once dehydroxylated, the composition of ES-NH is referable to the binary system  $Al_2O_3-SiO_2$  (circle marked E'' in Figure 5). To evaluate the approximation of this plot, it can be noted that the sum of oxides not belonging to the system corresponds to 2.66, 2.78, and 2.84 wt % for ES-NH dehydrated, de-ammoniated and dehydroxylated, respectively (Table 4). These approximations are in line with those common in evaluating raw materials for the ceramic industry [36] (p. 193). Being substantially constituted by a clinoptilolite with a Si/Al ratio = 4.71, ES-NH has a Si/Al ratio = 4.53, hence the points relative to this material (E, E', E'' in Figure 5) fall above the line corresponding to Si/Al = 4, used to distinguish heulandite (Si/Al ratio < 4) from clinoptilolite [37]. Moreover, the point E is located close to the line connecting the theoretical compositions of zeolites in  $NH_4$ -form, thus confirming that a near-end-member of  $NH_4$ -clinoptilolite was obtained. The point E' in Figure 5 ideally corresponds to ES-NH after ammonia evolution, i.e., to a material containing clinoptilolite in H-form [33]. After dehydroxylation, the chemistry of ES-NH reaches the composition  $SiO_2 = 84.1$  wt %;  $Al_2O_3 = 15.9$  wt % (E'' in Figure 5). In the binary system silica-alumina reported by Manning [36] (p. 191), this composition falls in the field of "fireclays", raw materials that are used to produce acid refractories constituted by an association of mullite and cristobalite. In the  $Al_2O_3-SiO_2$  system the eutectic temperature is 1590 °C, but the impurities in ES-NH (2.84 wt %; Table 4) determine the formation of a liquid phase at about 1200 °C, as shown by the thermal analyses (Figure 3).

An association constituted by mullite and amorphous silica was obtained by thermal treatment of two synthetic zeolites (X and LTA), previously  $NH_4$ -exchanged [12,13]. Among zeolites, LTA has the lowest Si/Al ratio (Si/Al = 1). In the diagram of Figure 5 the compositional variation of a  $NH_4$ -LTA zeolite after dehydration, de-ammoniation and dehydroxylation is reported. The same compositional

pathways were drawn for the two ammonium forms at the limits of the heulandite-clinoptilolite series, having Si/Al ratios of 2.6 and 5.7, respectively [38]. Once amorphized, all the zeolites reported in the diagram of Figure 5 reach compositions that, on the silica-alumina side, correspond to the field of “fireclays” [36] (p. 191).

By comparing the results of the present research with the data reported by Kosanovic et al. [12], it can be deduced that the Si/Al ratio affects the temperature of mullite nucleation and the kinetics of the transformation. In fact, NH<sub>4</sub>-exchanged LTA (Si/Al = 1) and X (Si/Al = 1.22) synthetic zeolites complete the reaction after 3 h at 1000 °C [12], whereas the NH<sub>4</sub>-clinoptilolite contained in ES-NH (Si/Al = 4.71) requires a treatment of 32 h at 1100 °C. This hypothesis is reinforced by the thermal behavior of a NH<sub>4</sub>-clinoptilolite with a Si/Al ratio of 5.01 which, heated for 2 h at 1100 °C, was not transformed to crystalline phases [23], and the same result was obtained after a 3 h treatment at 1000 °C of a NH<sub>4</sub>-mordenite with a Si/Al ratio of 4.35 [12].

The general reaction that leads to the formation of mullite and silica polymorphs from NH<sub>4</sub>-clinoptilolite can be summarized as:



with  $x$  that spans from 5.4 to 7.2 (and from 5.4 to 10 by considering the whole heulandite–clinoptilolite series) [38].

From the data in Table 4, with a simple proportion it is possible to calculate that the percentage of Al<sub>6</sub>Si<sub>2</sub>O<sub>13</sub> theoretically obtainable from ES-NH corresponds to 21.5 wt %. This value is consistent with the highest content determined through XRD analysis (21.8 wt %, Table 3). On the other hand, mullite shows various Si/Al ratios referring to the solid solution Al<sub>4+2x</sub>Si<sub>2-2x</sub>O<sub>10</sub>, with  $x$  ranging between about 0.2 and 0.9, and its structure is able to incorporate a number of transition metal cations and other foreign atoms [14]. Hence, the percentage of mullite (impure) could be slightly higher than the amount calculated on the basis of the theoretical formula Al<sub>6</sub>Si<sub>2</sub>O<sub>13</sub>. Moreover, crystalline phases, having formulae that deviate from ideal compositions, were already obtained by thermal treatment of synthetic zeolites [39] or clinoptilolite [21,22].

Previous studies demonstrated that some zeolite-rich rocks can be used to partially substitute the feldspathic fluxes commonly employed in porcelain stoneware production, though a dark color represents a frequent drawback [15,16,19]. In general, clinoptilolite-rich rocks have evidenced better performances with respect to those containing other natural zeolites, like phillipsite and chabazite [15]. The results of this research are interesting, because they indicate that NH<sub>4</sub>-clinoptilolite might represent a raw material of potential interest in the ceramic field, in particular in the production of acid refractory. Above all, it should be considered that clinoptilolite is a cheap commodity employable in NH<sub>4</sub><sup>+</sup> decontamination [1,8], and such a process would provide a material that can be transformed to an association of mullite and silica polymorphs, which means finding a way to turn waste into a resource. Finally, the synthesized matrix shows a whitish color (Figure S3, Supplementary Materials), a valuable feature in the ceramic field.

Further investigations should clarify the lowest clinoptilolite content and the minimum ammonium content necessary to obtain the transformation from NH<sub>4</sub>-clinoptilolite to mullite and silica polymorphs.

**Supplementary Materials:** The following are available online at [www.mdpi.com/2075-163X/7/1/11/s1](http://www.mdpi.com/2075-163X/7/1/11/s1). Figure S1: Experimental (blue) and calculated (red) X-ray powder diffraction pattern for ES-AR. Figure S2: Experimental (blue) and calculated (red) X-ray powder diffraction pattern for ES-NH heated for 32 h at 1100 °C. Figure S3: Sample of ES-NH recovered after the thermal analysis (air flow).

**Acknowledgments:** This work was partially financed by the Fund “Analisi Mineralogiche Cerri”, provided by Guido Cerri. Authors are grateful to two anonymous reviewers whose observations have improved the manuscript.

**Author Contributions:** Antonio Brundu and Guido Cerri conceived and designed the experiments; Antonio Brundu and Eleonora Sale performed all the experiments, except for the thermal analyses, executed by Guido Cerri; Antonio Brundu and Guido Cerri analyzed the data; Guido Cerri provided reagents/materials/analysis tools; Antonio Brundu and Guido Cerri wrote the manuscript.

**Conflicts of Interest:** The authors declare no conflict of interest.

## References

1. Eyde, T.H.; Holmes, D.A. Zeolites. In *Industrial Minerals and Rocks: Commodities, Markets, and Uses*, 7th ed.; Kogel, J.E., Trivedi, N.C., Barker, J.M., Krukowski, S.T., Eds.; Society for Mining, Metallurgy, and Exploration, Inc.: Littleton, CO, USA, 2006; pp. 1039–1064.
2. Pabalan, R.; Bertetti, F.P. Cation-Exchange Properties of Natural Zeolites. In *Natural Zeolites: Occurrence, Properties, Applications—Reviews in Mineralogy and Geochemistry*, 1st ed.; Bish, D.L., Ming, D.W., Eds.; Mineralogical Society of America: Washington, DC, USA, 2001; Volume 45, pp. 453–518.
3. Jorgensen, T.C.; Weatherley, L.R. Ammonia removal from wastewater by ion exchange in the presence of organic contaminants. *Water Res.* **2003**, *37*, 1723–1738. [[CrossRef](#)]
4. Sprynskyy, M.; Lebedynets, M.; Terzyk, A.P.; Kowalczyk, J.; Namieśnik, J.; Buszewski, B. Ammonium sorption from aqueous solutions by the natural zeolite Transcarpathian clinoptilolite studied under dynamic conditions. *J. Colloid Interface Sci.* **2005**, *284*, 408–415. [[CrossRef](#)] [[PubMed](#)]
5. Mazloomi, F.; Jalali, M. Ammonium removal from aqueous solutions by natural Iranian zeolite in the presence of organic acids, cations and anions. *J. Environ. Chem. Eng.* **2016**, *4*, 240–249. [[CrossRef](#)]
6. Virta, R.L.; Flanagan, D.M. Zeolites. In *Minerals Yearbook 2014*; U.S. Geological Survey: Reston, VA, USA, 2015; Volume 1, pp. 83.1–83.3.
7. Flanagan, D.M. Zeolites. In *Mineral Commodity Summaries 2016*; U.S. Geological Survey: Reston, VA, USA, 2016; pp. 190–191.
8. Armbruster, T. Clinoptilolite-heulandite: Applications and basic research. *Stud. Surf. Sci. Catal.* **2001**, *135*, 13–27.
9. Liberti, L.; Boghetich, G.; Lopez, A.; Petruzzelli, D. Application of microporous materials for the recovery of nutrients from wastewaters. In *Natural Microporous Materials in Environmental Technology—Nato Science Series*, 1st ed.; Misaelides, P., Macásek, F., Pinnavaia, T.J., Colella, C., Eds.; Springer Science & Business Media, B.V.: Dordrecht, The Netherlands, 1999; Volume 362, pp. 253–270.
10. Cruciani, G. Zeolites upon heating: Factors governing their thermal stability and structural changes. *J. Phys. Chem. Solids* **2006**, *67*, 1973–1994. [[CrossRef](#)]
11. Matsumoto, T.; Goto, Y.; Urabe, K. Formation process of mullite from  $\text{NH}_4^+$ -exchanged Zeolite A. *J. Ceram. Soc. Jpn.* **1995**, *103*, 93–95. [[CrossRef](#)]
12. Kosanović, C.; Subotić, B.; Smit, I. Thermally induced phase transformations in cation-exchanged zeolites 4A, 13X and synthetic mordenite and their amorphous derivatives obtained by mechanochemical treatment. *Thermochim. Acta* **1998**, *317*, 25–37. [[CrossRef](#)]
13. Kosanović, C.; Subotić, B. Preparation of mullite micro-vessels by a combined treatment of zeolite A. *Microporous Mesoporous Mater.* **2003**, *66*, 311–319. [[CrossRef](#)]
14. Schneider, H.; Schreuer, J.; Hildmann, B. Structure and properties of mullite—A review. *J. Eur. Ceram. Soc.* **2008**, *28*, 329–344. [[CrossRef](#)]
15. De Gennaro, R.; Cappelletti, P.; Cerri, G.; de' Gennaro, M.; Dondi, M.; Guarini, G.; Langella, A.; Naimo, D. Influence of zeolites on the sintering and technological properties of porcelain stoneware tiles. *J. Eur. Ceram. Soc.* **2003**, *23*, 2237–2245. [[CrossRef](#)]
16. De Gennaro, R.; Dondi, M.; Cappelletti, P.; Cerri, G.; de' Gennaro, M.; Guarini, G.; Langella, A.; Parlato, L.; Zanelli, C. Zeolite-feldspar epiclastic rocks as flux in ceramic tile manufacturing. *Microporous Mesoporous Mater.* **2007**, *105*, 273–278. [[CrossRef](#)]
17. Demirkiran, A.S.; Artir, R.; Avci, E. Effect of natural zeolite addition on sintering kinetics of porcelain bodies. *J. Mater. Process. Tech.* **2008**, *203*, 465–470. [[CrossRef](#)]
18. Ergul, S.; Sappa, G.; Magaldi, D.; Piscicella, P.; Pelino, M. Microstructural and phase transformations during sintering of a phillipsite rich zeolitic tuff. *Ceram. Int.* **2011**, *37*, 1843–1850. [[CrossRef](#)]
19. Sokolář, R.; Šveda, M. The use of zeolite as fluxing agent for whitewares. *Procedia Eng.* **2016**, *151*, 229–235. [[CrossRef](#)]

20. Brundu, A.; Cerri, G. Thermal transformation of Cs-clinoptilolite to CsAlSi<sub>5</sub>O<sub>12</sub>. *Microporous Mesoporous Mater.* **2015**, *208*, 44–49. [[CrossRef](#)]
21. Gatta, G.D.; Brundu, A.; Cappelletti, P.; Cerri, G.; de' Gennaro, B.; Farina, M.; Fumagalli, P.; Guaschino, L.; Lotti, P.; Mercurio, M. New insights on pressure, temperature, and chemical stability of CsAlSi<sub>5</sub>O<sub>12</sub>, a potential host for nuclear waste. *Phys. Chem. Miner.* **2016**, *43*, 639–647. [[CrossRef](#)]
22. Brundu, A.; Cerri, G. Release of lead from Pb-clinoptilolite: managing the fate of an exhausted exchanger. *Int. J. Environ. Sci. Technol.* **2016**. [[CrossRef](#)]
23. Tomazović, B.; Čeranić, T.; Sijarić, G. The properties of the NH<sub>4</sub>-clinoptilolite. Part 2. *Zeolites* **1996**, *16*, 309–312. [[CrossRef](#)]
24. Andreola, F.; Barbieri, L.; Karamanova, E.; Lancellotti, I.; Pelino, M. Recycling of CRT panel glass as fluxing agent in the porcelain stoneware tile production. *Ceram. Int.* **2008**, *34*, 1289–1295. [[CrossRef](#)]
25. Dondi, M.; Guarini, G.; Raimondo, M.; Zanelli, C. Recycling PC and TV waste glass in clay bricks and roof tiles. *Waste Manag.* **2009**, *29*, 1945–1951. [[CrossRef](#)] [[PubMed](#)]
26. Andreola, F.; Barbieri, L.; Lancellotti, I.; Leonelli, C.; Manfredini, T. Recycling of industrial wastes in ceramic manufacturing: State of art and glass case studies. *Ceram. Int.* **2016**, *42*, 13333–13338. [[CrossRef](#)]
27. Cerri, G.; Cappelletti, P.; Langella, A.; de' Gennaro, M. Zeolitization of Oligo-Miocene volcanoclastic rocks from Logudoro (northern Sardinia, Italy). *Contrib. Mineral. Petrol.* **2001**, *140*, 404–421. [[CrossRef](#)]
28. Cerri, G.; de' Gennaro, M.; Bonferoni, M.C.; Caramella, C. Zeolites in biomedical application: Zn-exchanged clinoptilolite-rich rock as active carrier for antibiotics in anti-acne topical therapy. *Appl. Clay Sci.* **2004**, *27*, 141–150. [[CrossRef](#)]
29. Brundu, A.; Cerri, G.; Colella, A.; de Gennaro, M. Effects of thermal treatments on Pb-clinoptilolite. *Rend. Online Soc. Geol. Italy* **2008**, *3*, 138–139.
30. Cerri, G.; Farina, M.; Brundu, A.; Daković, A.; Giunchedi, P.; Gavini, E.; Rassa, G. Natural zeolites for pharmaceutical formulations: Preparation and evaluation of a clinoptilolite-based material. *Microporous Mesoporous Mater.* **2016**, *223*, 58–67. [[CrossRef](#)]
31. Kesraoul-Oukl, S.; Cheeseman, C.; Perry, R. Effects of conditioning and treatment of chabazite and clinoptilolite prior to lead and cadmium removal. *Environ. Sci. Technol.* **1993**, *27*, 1108–1116. [[CrossRef](#)]
32. Tomazović, B.; Čeranić, T.; Sijarić, G. The properties of the NH<sub>4</sub>-clinoptilolite. Part 1. *Zeolites* **1996**, *16*, 301–308. [[CrossRef](#)]
33. Jacobs, P.A.; Uytterhoeven, J.B.; Beyer, H.K.; Kiss, A. Preparation and Properties of Hydrogen Form of Stilbite, Heulandite and Clinoptilolite Zeolites. *J. Chem. Soc. Faraday Trans. 1* **1979**, *75*, 883–891. [[CrossRef](#)]
34. Langella, A.; Pansini, M.; Cerri, G.; Cappelletti, P.; de Gennaro, M. Thermal behavior of natural and cation-exchanged clinoptilolite from Sardinia (Italy). *Clays Clay Min.* **2003**, *51*, 625–633. [[CrossRef](#)]
35. Stoch, L.; Waclawska, I. Phase Transformations in Amorphous Solids. *High Temp. Mater. Proc.* **1994**, *13*, 181–201. [[CrossRef](#)]
36. Manning, D.A.C. *Introduction to Industrial Minerals*, 1st ed.; Chapman & Hall: London, UK, 1995; p. 276.
37. Coombs, D.S.; Alberti, A.; Armbruster, T.; Artioli, G.; Colella, C.; Galli, E.; Grice, J.D.; Liebau, F.; Mandarino, J.A.; Minato, H.; et al. Recommended nomenclature for zeolite minerals: Report of the Subcommittee on Zeolites of the International Mineralogical Association, Commission on New Minerals and Mineral Names. *Can. Miner.* **1997**, *35*, 1571–1606.
38. Bish, D.L.; Boak, J.M. Clinoptilolite-Heulandite Nomenclature. In *Natural Zeolites: Occurrence, Properties, Applications—Reviews in Mineralogy and Geochemistry*, 1st ed.; Bish, D.L., Ming, D.W., Eds.; Mineralogical Society of America: Washington, DC, USA, 2001; Volume 45, pp. 207–216.
39. Radosavljevic-Mihajlovic, A.S.; Kremenovic, A.S.; Dosen, A.M.; Andrejic, J.Z.; Dondur, V.T. Thermally induced phase transformation of Pb-exchanged LTA and FAU-framework zeolite to feldspar phases. *Microporous Mesoporous Mater.* **2015**, *201*, 210–218. [[CrossRef](#)]

